Supplementary information:

Electron paramagnetic resonance and electric characterization of [CH₃NH₂NH₂][Zn(HCOO)₃] perovskite metal formate framework

Mantas Šimėnas,[1] Sergejus Balčiūnas,[1] Monika Trzebiatowska,[2] Maciej Ptak,[2] Mirosław Mączka,[2] Georg Völkel,[3] Andreas Pöppl,[3] and Jūras Banys[1]

[1] Faculty of Physics, Vilnius University, Saulėtekio 9, LT-10222 Vilnius, Lithuania

[2] Institute of Low Temperature and Structure Research, Polish Academy of Sciences, P.O. Box-1410, PL-50-950 Wroclaw 2, Poland

[3] Faculty of Physics and Earth Sciences, Universität Leipzig, Linnestrasse 5, D-04103 Leipzig, Germany

1

Electric Polarization
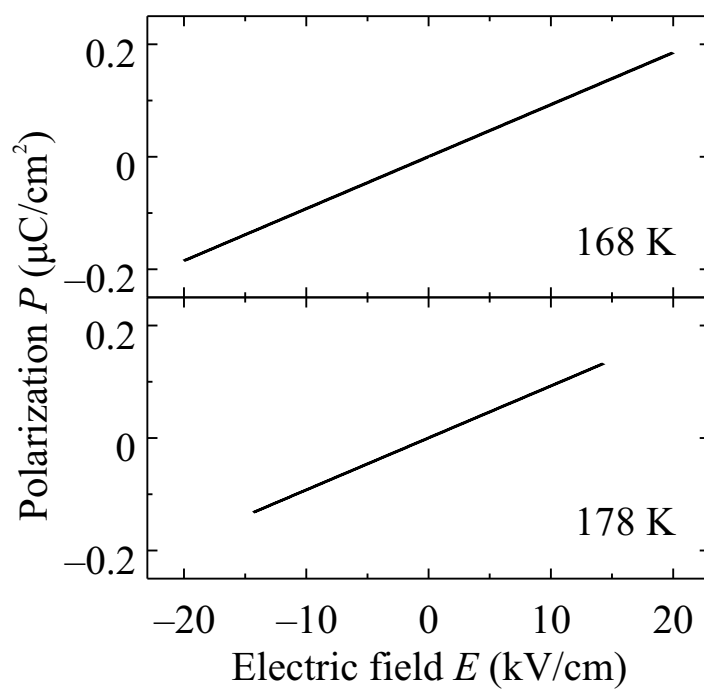
Figure S1: Electric field dependence of the electric polarization of **1** obtained along the axis perpendicular to the (035) plane at 168 and 178 K.

Additional Dielectric Spectroscopy Data
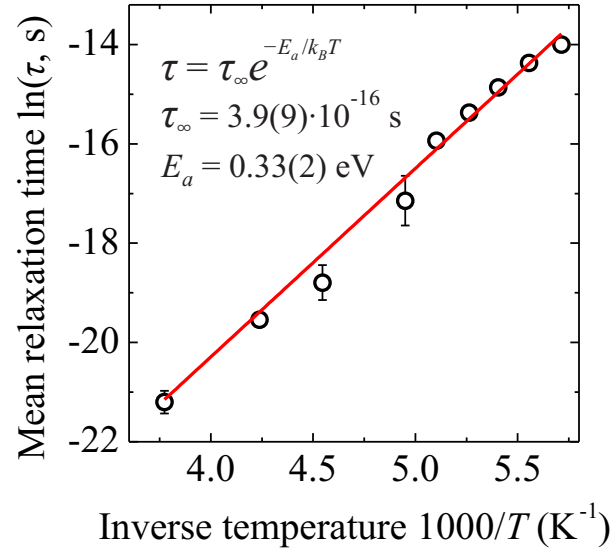
Figure S2: Inverse temperature dependence of the mean relaxation time. The observed linear behavior indicates Arrhenius-type temperature dependence: $\tau = \tau_\infty e^{-E_a/k_B T}$, where the activation energy $E_a = 0.33(2)$ eV and the attempt relaxation time $\tau_\infty = 3.9(9) \times 10^{-16}$ s.

Additional EPR Data
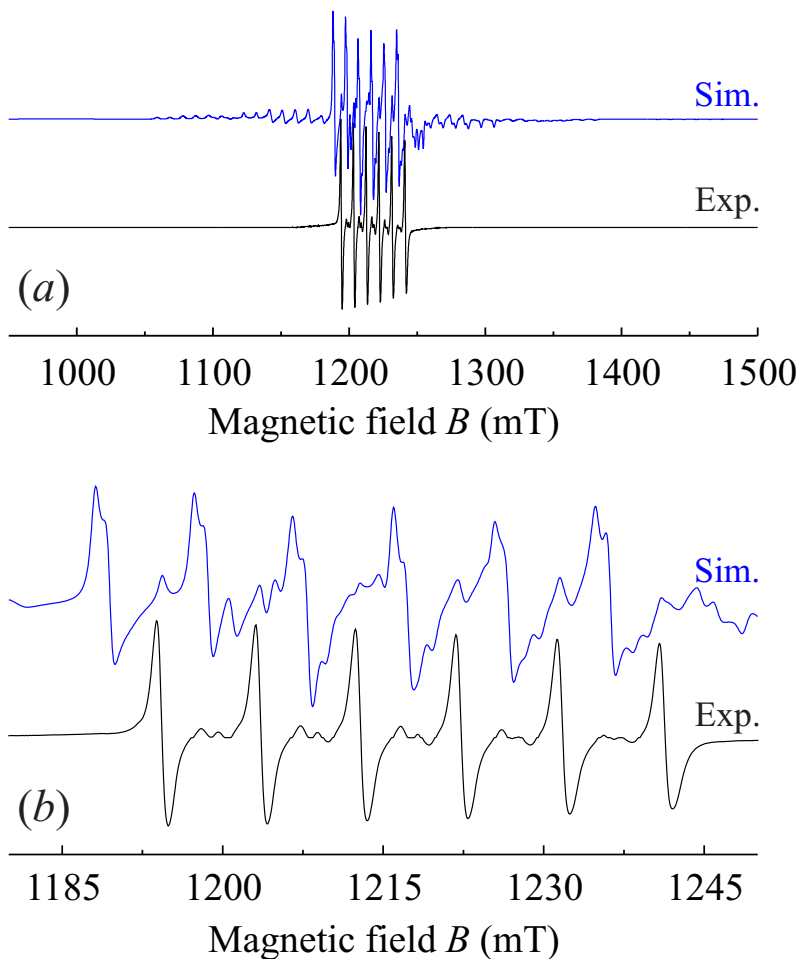
Figure S3: (a) Simulated Q-band spectrum using $g = 2.0002$, $A_{\mathrm{iso}} = -262$ MHz, $D = 1.8$ GHz and $E = 100$ MHz. The experimental spectrum of **2** is presented for comparison. In (b) the central fs transition is enlarged indicating a clear mismatch of the hf lines in comparison with the experiment. A clear discrepancy between the simulated and experimental spectra indicates that such spin Hamiltonian parameters are unsuitable to describe the main Mn^{2+} species in **2**.
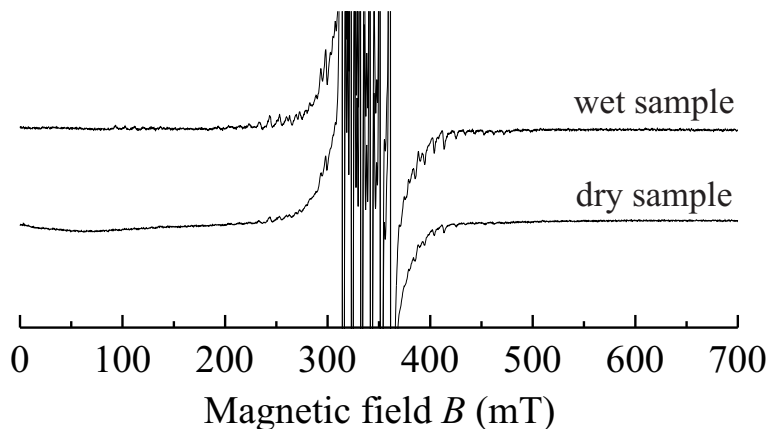
Figure S4: Normalized room temperature X-band CW EPR spectra of manganese doped MHyZnF compound kept under dry and afterwards under wet conditions. Note the much stronger intensity of impurity Mn^{2+} species in the wet sample.
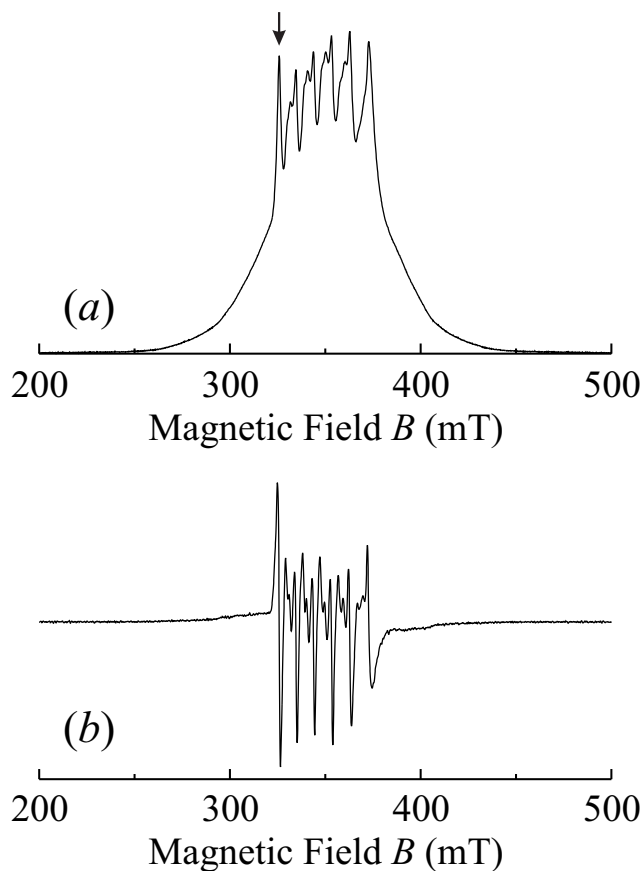
Figure S5: (a) Two-pulse echo-detected field-sweep pulse EPR spectrum of **2** recorded at 25 K. (b) The corresponding first derivative spectrum. The arrow in (a) marks position at which the ESEEM, ENDOR and relaxation time measurements were performed.
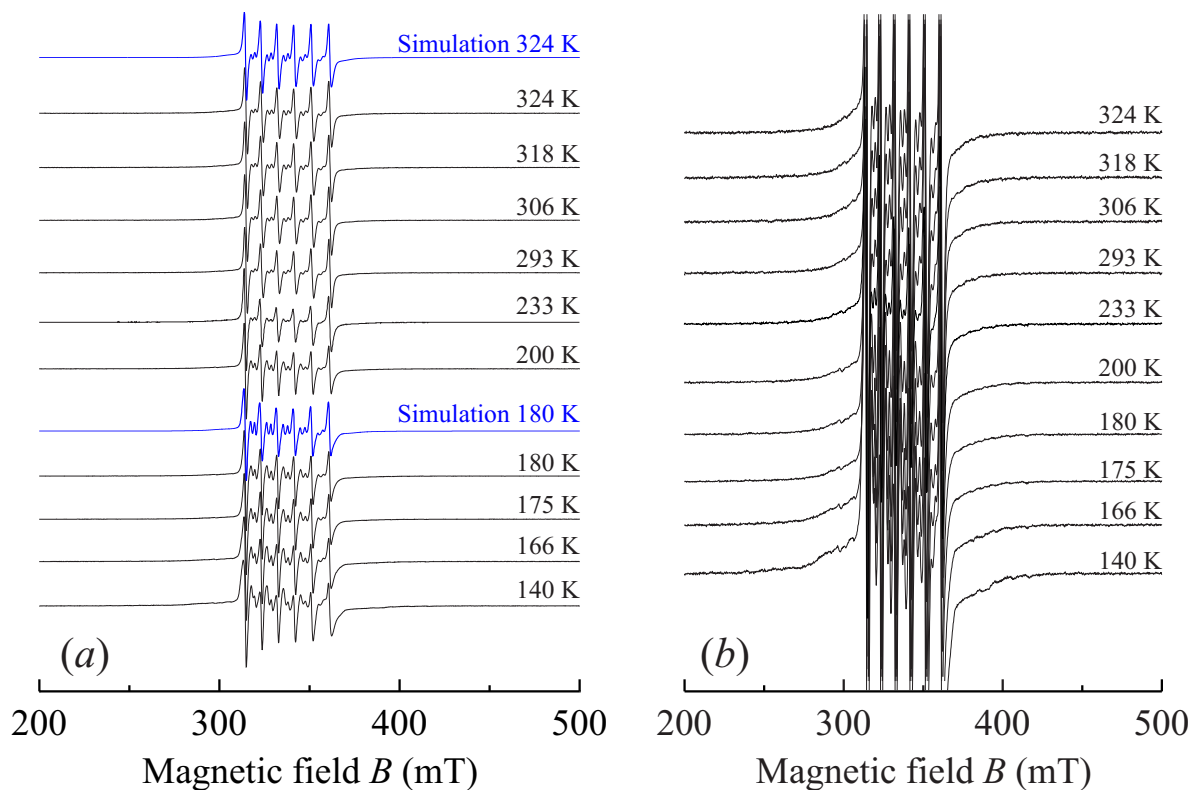
Figure S6: Normalized temperature dependent X-band spectra of **2**. Emphasis on (a) central and (b) outer transitions. Simulation of the 324 K spectrum is also presented in (a).
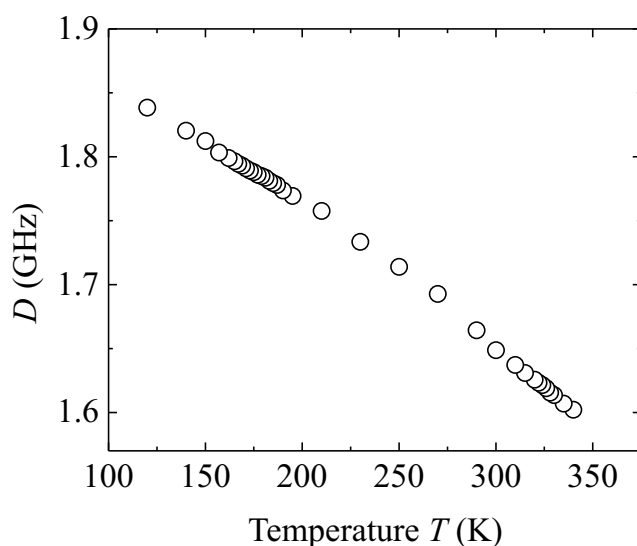
Figure S7: Temperature dependence of the axial zfs parameter of the impurity Mn^{2+} species of **2**. The values of D were estimated from the width of the fs. Error bars are smaller than data points.
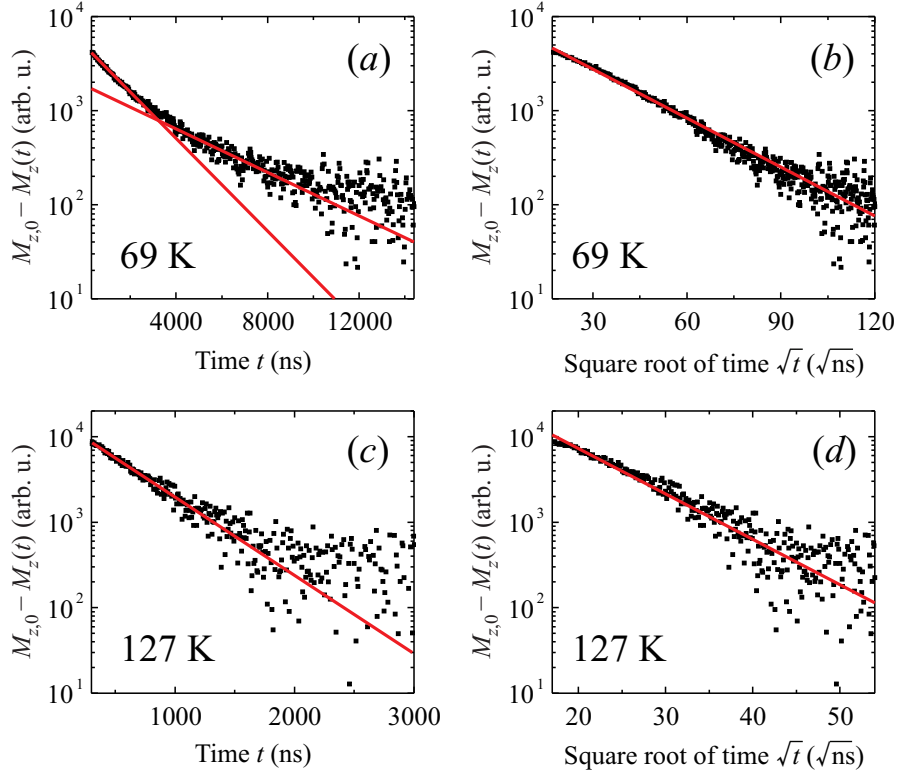
Figure S8: The kinetics of the longitudinal magnetization recovery of Mn^{2+} ions in **2**. The recovery is two-exponential at (a) 67 K, while it is single exponential at (b) 127 K. In (b) and (d) the corresponding magnetization kinetics are scaled by $\sqrt{t}$.
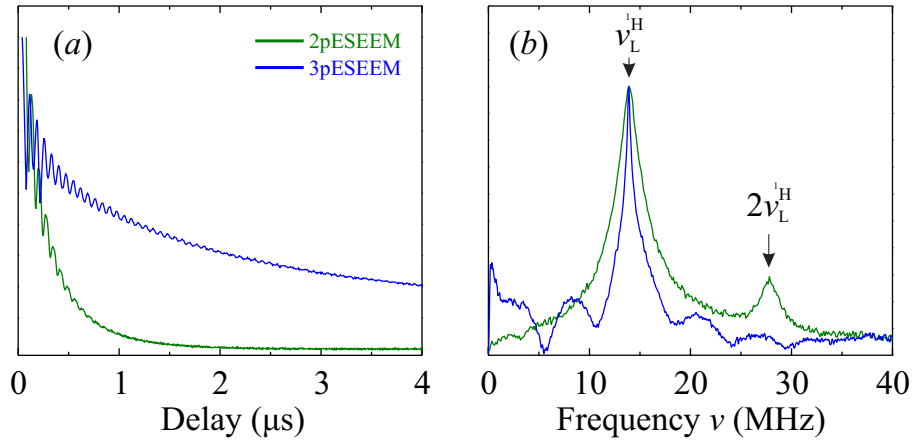
Figure S9: (a) Time and (b) frequency domain patterns of the two-pulse and three-pulse ESEEM experiments of **2** obtained at 25 K and 325 mT. In (b) the proton Larmor frequency and its double value are indicated by the arrows.
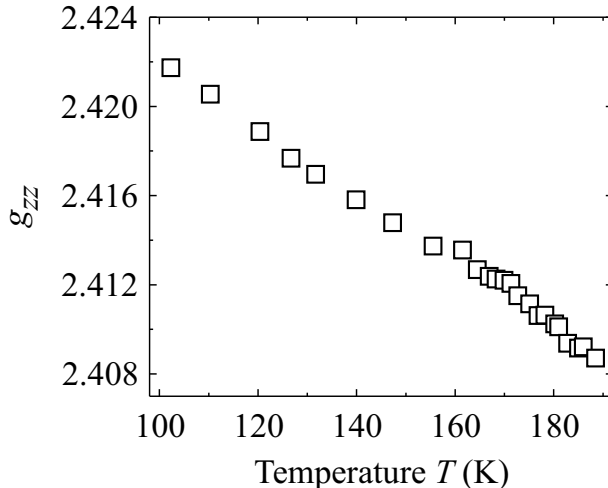
Figure S10: Temperature dependence of $g_{zz,2}$ of **3**. Errors bars are approximately of the same size as the data points.

IR and Raman data

Low-frequency temperature-dependent Raman spectra of **2** were measured using a Renishaw InVia Raman spectrometer equipped with a confocal DM 2500 Leica optical microscope, a thermoelectrically cooled CCD as a detector, Eclipse filter, a diode laser operating at 830 nm and a Linkam cryostat cell THMS600. Far-IR temperature-dependent IR spectra were measured using a Biorad 575C FT-IR spectrometer and a helium-flow Oxford cryostat. The spectral resolution of Raman and IR spectra was 2 cm^{-1}.

Temperature-dependent Raman and IR spectra of **2** are presented in Figures S10 and S11. Among the observed bands, only those observed near 440 and 270 cm^{-1} can be attributed to internal modes, i.e., δ(CNN) and τ(CH3) modes. The remaining bands correspond to the lattice modes, that is, translations of MHy$^+$, HCOO$^-$ and Zn^{2+}/Mn^{2+} cations as well as librational motions of MHy$^+$ and HCOO$^-$ cations. Lattice dynamic calculations performed for related $[(CH_3)_2NH_2][Ni(HCOO)_3]$ framework compound showed that the lattice modes are strongly coupled.[1] Nevertheless, we propose assignment of the lattice modes of **2** based on some observations of Raman and IR spectra for related framework compounds.[2–4] Firstly, librational modes of the HCOO$^-$ ions give rise to strong Raman and weak IR bands whereas

8

opposite behavior is observed for T'(HCOO$^-$) modes. Secondly, librational and translational modes of protonated amines are observed as weak bands, usually below 200 cm^{-1}. Thirdly, translations of divalent cations contribute significantly to the modes observed in the 200-400 cm^{-1} range.

Temperature-dependent spectra show three major features upon cooling. Firstly, Raman and IR bands remain broad down to 180 K but exhibit strong narrowing below 160 K. Secondly, many bands split at low temperature into a few components and some additional weak bands appear. Thirdly, all bands exhibit hardening with decrease of temperature in the 300-180 K range and softening as T_{c2} is approached from below. The narrowing and splitting of bands confirms that **2** undergoes an order-disorder phase transition associated with significant decrease of symmetry. Lack of any pronounced softening upon cooling is also consistent with an order-disorder character of the phase transition.
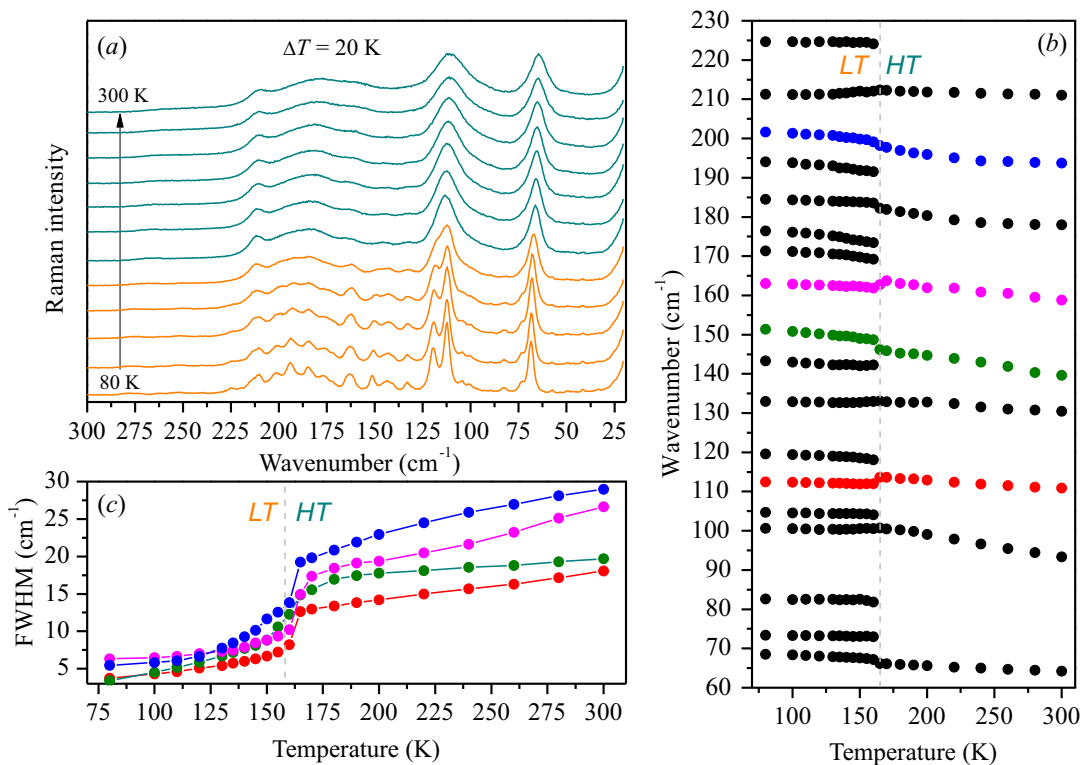
Figure S11: (a) Temperature-dependent Raman spectra of **2** in the 30-300 cm^{-1} range, (b) temperature dependence of selected Raman wavenumbers and (c) temperature dependence of FWHM for the 194 cm^{-1} (blue), 159 cm^{-1} (magenta), 140 cm^{-1} (green) and 111 cm^{-1} (red) Raman bands.
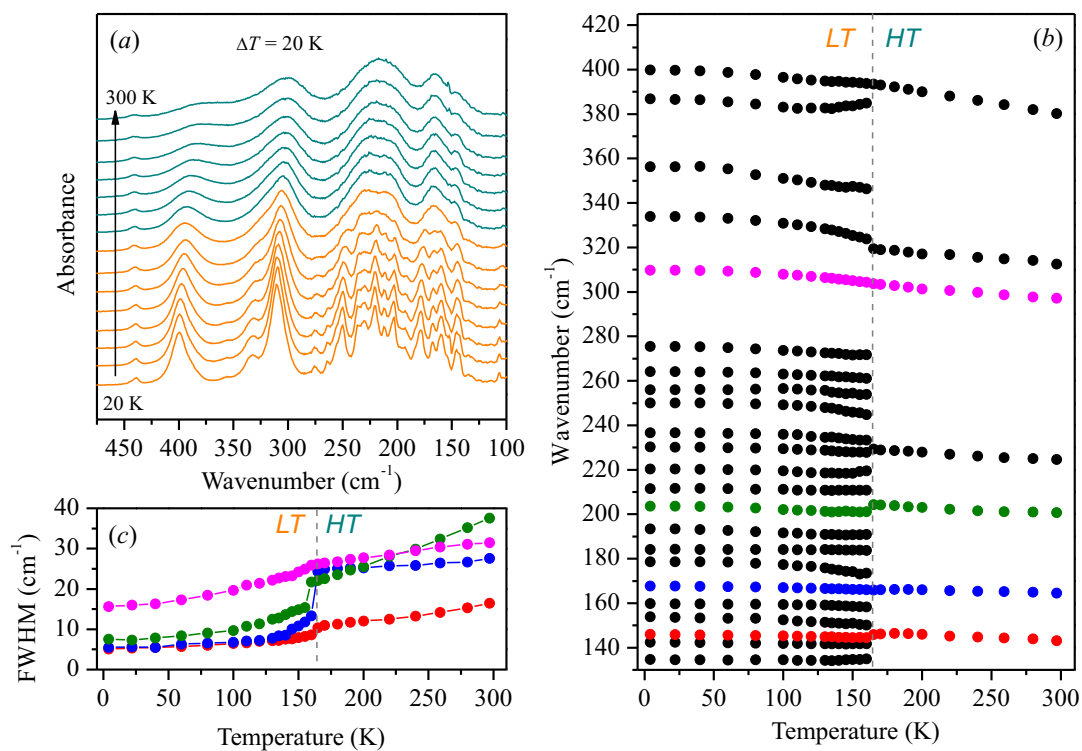
Figure S12: (a) Temperature-dependent IR spectra of **2** in the 100-475 cm^{-1} range, (b) temperature dependence of selected IR wavenumbers and (c) temperature dependence of FWHM for the 297 cm^{-1} (magenta), 201 cm^{-1} (green), 164 cm^{-1} (blue) and 143 cm^{-1} (red) bands.

11

References

(1) Mączka, M.; Zierkiewicz, W.; Michalska, D.; Hanuza, J. Vibrational Properties and DFT Calculations of the Perovskite Metal Formate Framework of $[(CH_3)_2NH_2][Ni(HCOO_3)]$ System. *Spectrochimica Acta Part A: Molecular and Biomolecular Spectroscopy* **2014**, *128*, 674 – 680.

(2) Mączka, M.; Ptak, M.; Macalik, L. Infrared and Raman Studies of Phase Transitions in Metal-Organic Frameworks of $[(CH_3)_2NH_2][M(HCOO)_3]$ with M=Zn, Fe. *Vibrational Spectroscopy* **2014**, *71*, 98–104.

(3) Mączka, M.; Pietraszko, A.; Macalik, B.; Hermanowicz, K. Structure, Phonon Properties, and Order-Disorder Transition in the Metal Formate Framework of $[NH_4][Mg(HCOO)_3]$. *Inorganic Chemistry* **2014**, *53*, 787–794.

(4) Mączka, M.; Ciupa, A.; Gagor, A.; Sieradzki, A.; Pikul, A.; Macalik, B.; Drozd, M. Perovskite Metal Formate Framework of $[NH_2-CH^+-NH_2]Mn(HCOO)_3$: Phase Transition, Magnetic, Dielectric, and Phonon Properties. *Inorganic Chemistry* **2014**, *53*, 5260–5268.